Available online at www.sciencedirect.com
ScienceDirect
Scripta Materialia 63 (2010) 8–11
Scripta MATERIALIA
www.elsevier.com/locate/scriptamat

Incorporating diffuse-interface nuclei in phase-field simulations

Tae Wook Heo,[a,*] Lei Zhang,[b,1] Qiang Du[a,b] and Long-Qing Chen[a]

[a] *Department of Materials Science and Engineering, The Pennsylvania State University, University Park, PA 16802, USA*
[b] *Department of Mathematics, The Pennsylvania State University, University Park, PA 16802, USA*

Received 9 February 2010; revised 14 February 2010; accepted 15 February 2010
Available online 18 February 2010

We propose a computational framework for incorporating diffuse-interface critical nuclei in phase-field simulations. Using a structural transformation as an example, we first generate a table of diffuse-interface critical nuclei. We then incorporate them in phase-field simulations through the explicit nucleation algorithm. The temporal growth kinetics of the introduced nuclei is obtained by numerically solving the Allen–Cahn equation. The results are analyzed by comparing to the phase transformation kinetics using the classical nucleation and normal growth theory and the Kolmogorov–Johnson–Mehl–Avrami equation.

Keywords: Diffuse-interface critical nuclei; Nucleation of phase transformations; Growth kinetics; Phase-field model

The phase-field method has been used to model microstructure evolution for many different materials processes [1–6]. In most phase-field simulations, the phase-field equations are deterministic with the evolution of the phase-field variables being driven by the reduction in the total free energy of an inhomogeneous system. However, many of the materials processes such as phase transformations take place through a nucleation and growth process so that it is crucial to effectively simulate such a process within the phase-field framework. Existing approaches of treating nucleation in phase-field method can be separated into two types, one being the introduction of Langevin noise [7,8] and the other the explicit nucleation method [9,10]. In the Langevin noise method, stochastic phase-field equations are solved. The method works well when the initial state is not too far away from the instability temperature or composition with respect to its transformation to the new state, i.e., the metastability of the parent phase is small. It is very difficult to induce nucleation events if a system is highly metastable unless the amplitude of noise is unrealistically large; moreover, the number of particles nucleated also depends on the amplitude and spatial correlation of the noise [11–14]. On the other hand, the explicit nucleation method is based on the classical nucleation theory [15] and Poisson seeding [16–18]. In this method, the critical size and critical free energy of formation of a nucleus are determined using the classical nucleation theory which assumes homogeneous properties within a critical nucleus and a sharp-interface between a nucleus and matrix. Whether or not a critical nucleus is introduced at a given location is determined by comparing a random number between 0.0 and 1.0 with the probability of nucleation. There are two main drawbacks of this approach. One is related to the conservation of mass for phase transformations involving composition changes. Since the composition of a new phase particle is different from the parent phase, the addition of a critical nucleus alters the overall composition. To conserve the overall composition, removal of solute atoms around an embedded nucleus is necessary. The second drawback has to do with the sharp-interface description between a critical nucleus and the parent matrix. Because of the diffuse-interface nature of phase-field method, introduction of a nucleus with sharp-interfaces requires relaxation from the highly non-equilibrium sharp-interface to the diffuse-interface dictated by the thermodynamics of the system. This can introduce artifacts in the kinetics of evolution during the nucleation stage.

In this work, we propose a new approach to treat nucleation in phase-field simulations which combines diffuse-interface theory of nucleation [19–21] with Poisson seeding. We first obtain the diffuse-interface critical profiles [22–25] employing either the minimax variational approach [26,27] or the constrained string method [28,29]. We then use the explicit nucleation process [9,10] for introducing critical nuclei in phase-field simulations.

* Corresponding author; e-mail: tuh134@psu.edu
[1] Present address: Department of Mathematics, University of California, Irvine, CA 92697, USA.

1359-6462/$ - see front matter © 2010 Acta Materialia Inc. Published by Elsevier Ltd. All rights reserved.
doi:10.1016/j.scriptamat.2010.02.028

Using the new approach, we predicted the morphological evolution and the kinetics for a phase transformation via homogeneous nucleation and normal growth. A similar approach was previously discussed in [30].

As a first attempt to implement diffuse-interface critical nuclei, we considered the simple case of structural transformation without compositional change in a two-dimensional system as an illustration. Following the studies in Refs. [22–25], our approach can be extended to include the contributions of the elastic energy, interfacial energy anisotropy effects, and composition change. The structural difference between the parent phase and the new phase is described by a single non-conserved order parameter η. The total free energy F is given by $F = \int_\Omega \left(f(\eta) + \frac{\kappa_o}{2}(\vec{\nabla}\eta)^2\right) d\vec{r}$ [19], where f is the local free energy density, κ_o is the gradient energy coefficient, and Ω represents the volume of the whole system.

We chose a simple double-well potential $f(\eta) = \frac{(\eta^2-1)^2}{4} + \frac{3}{4}\lambda\left(\frac{\eta^3}{3} - \eta\right)$ for the local free energy density to describe the structural phase transformation.

The bulk driving force for the phase transformation from the $\eta = -1$ state to $\eta = +1$ state is equal to λ. The increase of the total free energy caused by the order parameter fluctuation in an initial homogeneous state with η_0 is given by $\Delta F = \int_\Omega \left(\Delta f(\eta) + \frac{\kappa_o}{2}(\vec{\nabla}\eta)^2\right) d\vec{r}$, where $\Delta f(\eta) = f(\eta) - f(\eta_0)$. The critical nucleus is the order parameter fluctuation which has the total energy at the saddle point. In order to obtain the critical profiles describing a critical nucleus, we employed the minimax technique (see the details in Refs. [22–24]). The nuclei were generated numerically on a square domain discretized by a $64\Delta x \times 64\Delta x$ square grid which provided sufficient spatial resolution. The grid size is $\Delta x = 0.03$, and the gradient energy coefficient, $\kappa_o = 0.006$. The initial order parameter value for the parent phase was chosen to be -1. We computed critical nucleus profiles at different values of driving forces. Some examples of the critical profiles are shown in Figure 1a and b. The critical nucleation energy (ΔG^*) as a function of driving force is plotted in Figure 1c. As expected, the size of critical nuclei and the critical nucleation energy decrease with the increase of the driving force. The critical nucleation energy is non-dimensionalized by $k_B T$ where k_B is the Boltzman constant and T is the absolute temperature. The calculated diffuse-interface critical nucleation energy (ΔG^*) was compared with that from the classical nucleation theory [15] $\Delta G^* = \frac{\pi\sigma^2}{\lambda}$, where σ is the specific interfacial energy. The interfacial energy was calculated by the integration of excess energy across the interface when λ is equal to zero [19]

$$\sigma = \int_{-\infty}^{+\infty} \left(\Delta f(\eta) + \frac{\kappa_o}{2}(\vec{\nabla}\eta)^2\right) dx. \quad (1)$$

The calculated interfacial energy (σ) is 7.3×10^{-2}. As shown in Figure 1c, there is no significant difference in the calculated critical energy between the classical and the diffuse-interface nucleation theory.

We added one critical nucleus (with $\lambda = 0.1172$) to evaluate the growth kinetics of a single nucleus. The critical nucleus was embedded at the center of a square domain with $128\Delta x \times 128\Delta x$ grids. As shown in Figure 2a, the order parameter profile in the square area within the dashed line was replaced by that in the square domain (with $64\Delta x \times 64\Delta x$ grids) containing the critical nucleus. The cross-section profiles of the order parameter before and after the addition of a nucleus were plotted in Figure 2b.

The temporal evolution of order parameter was obtained using the Allen–Cahn equation [31]:

$$\frac{\partial\eta(\vec{r},t)}{\partial t} = -L\left(\frac{\delta F}{\delta\eta(\vec{r},t)}\right), \quad (2)$$

where L is the kinetic coefficient related to interfacial mobility, t is time, and $\left(\frac{\delta F}{\delta\eta}\right)$ is the variation of the free energy function with respect to the order parameter. The equations were solved by employing the finite difference method.

The values for Δx and κ_o are the same as those for generating the critical nuclei. The time step Δt was chosen to be 0.002, and L was 2.0. The particle growth is shown in Figure 3a. The radius of the growing particle as a function of time step was plotted in open circles in Figure 3b. The radius was calculated from the area of the transformed phase. The area of the transformed phase was obtained by counting the number of grid points having the order parameter value greater than zero. The growth rate increases as the particle grows due to the decrease of the Gibbs–Thomson effect without the change of λ. In order to elucidate the contributions of curvature and the driving force for phase transformation to the growth rate, we compare the kinetics of single diffuse-interface nucleus growth with

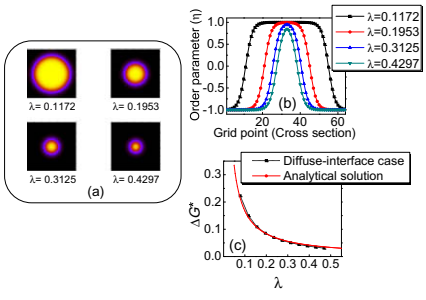

Figure 1. (a) Planar order parameter profiles of some examples of diffuse-interface critical nuclei, (b) their cross sections, and (c) the critical nucleation energy (ΔG^*) as a function of driving force (λ).

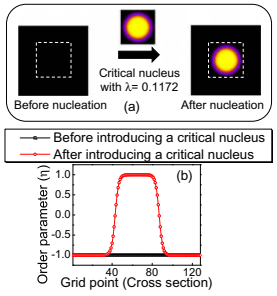

Figure 2. (a) The addition of a single diffuse-interface critical nucleus generated in a $64\Delta x \times 64\Delta x$ square domain to $128\Delta x \times 128\Delta x$ domain, and (b) the cross section of the order parameter profiles before and after the addition of a diffuse-interface critical nucleus.

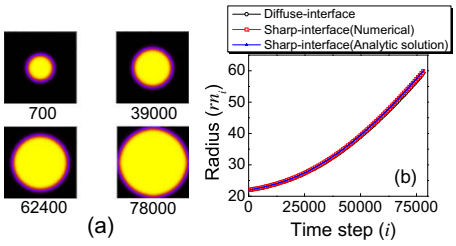

Figure 3. The temporal evolution of single nucleus growth. (a) The morphologies of the growing particle are at 700, 39,000, 62,400, and 78,000 time steps, and (b) the radius of the single growing particle as a function of time step.

that of single classical (sharp-interface) nucleus growth. In the case of the sharp-interface description for the growth of the nucleus, both the Gibbs–Thomson effect $\left(\frac{\sigma}{r}\right)$ and the driving force for phase transformation (Δg) have to be explicitly included:

$$\frac{dR}{dt} = M_r \cdot \left(\Delta g - \frac{\sigma}{R}\right), \tag{3}$$

where R is the radius of the growing particle, t is time, M_r is the mobility for the interface migration, Δg is the driving force for phase transformation, and σ is the interfacial energy. M_r and L are related by $M_r = \frac{\kappa \cdot L}{\sigma}$. [32].

The analytic equation for the relation between R and t can be obtained from Eq. (3) as the following:

$$\frac{1}{\Delta g}(R - R_0) + \frac{\sigma}{\Delta g^2} \ln\left[\frac{\Delta g \cdot R - \sigma}{\Delta g \cdot R_0 - \sigma}\right] = M_r \cdot t, \tag{4}$$

where R_0 is the initial radius of the particle. The values of R as a function of t from Eq. (4) are shown in a solid line in Figure 3b.

The differential equation (Eq. (3)) was also numerically solved to obtain the radius of the particle as a function of time. The explicit Euler scheme was employed to solve Eq. (3) as follows:

$$rn_{i+1} = rn_i + \Delta t \cdot \frac{M_r}{\Delta x}\left(\Delta g - \frac{\sigma}{rn_i \cdot \Delta x}\right), \tag{5}$$

where Δx is the spatial grid size, Δt is the time interval, and rn_i is the radius in a discretized system (i.e., $R = rn \cdot \Delta x$) at time step i. The values of Δx and Δt were taken to be the same as those in the phase-field simulation of diffuse-interface nucleus growth. The same interfacial energy (σ) was taken as that of the diffuse-interface calculated by Eq. (1).

The result from Eq. (5) was plotted in open squares in Figure 3b. First of all, the results numerically computed from Eq. (5) agree with the analytic equation (Eq. (4)). In addition, the agreement between the phase-field simulation result and results from Eq. (5) indicates that the Gibbs–Thomson effect was properly taken into account in the growth of diffuse-interface nucleus in the phase-field simulations.

The multiple nucleation events were conducted by the explicit nucleation algorithm developed by Simmons et al. [9,10]. We considered a $1024\Delta x \times 1024\Delta x$ square grid. First, one of $64\Delta x \times 64\Delta x$ square phase-field cells is randomly chosen by determining the middle point location of the phase-field cell in the whole domain using the uniformly distributed random numbers as a nucleation site. Given nucleation rate I, the nucleation probability P is given by $P = 1 - \exp(-I \cdot \Delta t)$, where Δt is the time interval between time steps. At the same time, a uniformly distributed random number between 0 and 1 is generated. If the probability is greater than the random number, a nucleus is added at the cell. The nucleation rate I is $I = I_0 \exp(-\Delta G^*)$, where I_0 is the prefactor and ΔG^* is the critical nucleation energy.

To avoid nucleation on the cells which are already transformed, the chosen $64\Delta x \times 64\Delta x$ cell for the potential nucleation is scanned. If any transformed grid points are found, the nucleation is not allowed to happen. The nucleation algorithm was implemented for every single time step. The driving force for the phase transformation between two states at $\eta = \pm 1$ was chosen to be 0.1172. The prefactor (I_0) for the nucleation rate was chosen to be 0.5, which leads to a nucleation rate of the order of 10^{-7}.

The temporal evolution of nucleation and growth process is shown in Figure 4a. The area fraction of the transformed phase as a function of time step is plotted in solid squares in Figure 4b. The area fraction was calculated by counting the number of grid points having the order parameter value greater than zero. We compared the simulation result with the Kolmogorov–Johnson–Mehl–Avrami (KJMA) equation $f(t) = 1 - \exp(X_e(t))$, [33–37] where $f(t)$ is the area fraction of the transformed phase at time t, and $X_e(t)$ is the extended area fraction of the transformed phase at time t. If the nucleation and growth rates are constant, the KJMA equation in two dimensions becomes a simple form as the following:

$$f(t) = 1 - \exp\left(-\frac{\pi \cdot I \cdot u^2}{3} t^3\right), \tag{6}$$

where I is the nucleation rate, u is the growth rate, and t is time. However, the growth rate is not constant as shown in the simulation of single nucleus growth in Figure 3b. Thus, Eq. (6) cannot be directly applied. The analytical form of the KJMA equation for the varying growth rate is generally not available except for simple time-dependences of the growth rates. Thus, we resort to numerical calculations. In the numerical scheme is expressed as $f(i) = 1 - \exp(X_e(i))$, where $f(i)$ is the area fraction of the transformed phase at time step i, and $X_e(i)$ is the extended area fraction of the transformed phase at time step i. According to the KJMA interpretation, the difference in the area fraction of the transformed phase between

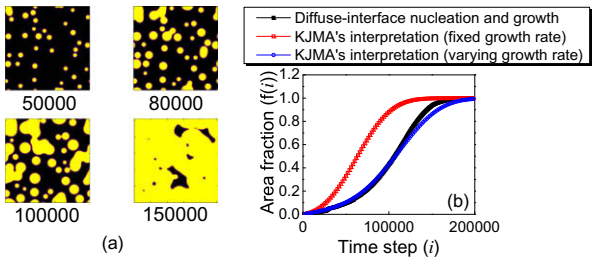

Figure 4. The temporal evolution of multiple nucleation events and growth. (a) The morphologies of growing particles are at 50,000, 80,000, 100,000, and 150,000 time steps, and (b) the area fraction of transformed phase as a function of time step.

time step i and $i+1$, is the summation of newly nucleated phase area fraction at time step i and the area fraction increase of existing transformed phase at time step i. At time step i, there exist nuclei with different radii. The radii include rn_k ($k = 0, \ldots, (i-1)$) where rn_k is the radius of a nucleus which is nucleated at time step $(i-k)$ and grows for k time intervals. For instance, rn_5 is the radius of a nucleus taking place at time step $(i-5)$ and growing for five time intervals. During one time interval, all the nuclei grow from the nuclei of rn_k to those of rn_{k+1} as well as new nuclei of radii rn_0 take place. Thus, the recurrence relation for $X_e(i)$ can be constructed as the following:

$$X_e(i+1) = X_e(i) + \frac{\left[I\cdot\Delta t\cdot\pi\cdot(rn_0\Delta x)^2 + I\cdot\Delta t\cdot\pi\sum_{k=0}^{i-1}((rn_{k+1}\Delta x)^2 - (rn_k\Delta x)^2)\right]}{(N_x\Delta x)\cdot(N_y\Delta x)} = X_e(i) + \frac{I\cdot\Delta t\cdot\pi\cdot(rn_i\Delta x)^2}{(N_x\Delta x)\cdot(N_y\Delta x)} \tag{7}$$

where I is the nucleation rate, Δx is the spatial grid size, N_x (=1024) is the total number of grid points along x direction, N_y (=1024) is the total number of grid points along y direction, and Δt is the time interval. The radius of nucleus at time step i (rn_i) can be obtained by the same scheme as Eq. (5). The area fraction of transformed phase as a function of time step calculated by the recurrence relation is plotted in open circles in Figure 4b. For comparison, the area fraction of transformed phase when the growth rate is constant (without including the Gibbs–Thomson effect in KJMA equation is plotted in open squares in Figure 4b. In the case of fixed growth rate in Figure 4b, the state at $\eta = -1$ is transformed to $\eta = +1$ faster than the case of variable growth rate. This is because the initial growth rate of a single nucleus is slower due to the Gibbs–Thomson effect.

The phase-field simulation result in Figure 4b agrees well with that from the recurrence relation except at later stages during which impingement takes place. In the KJMA equation, the impingement is considered simply by the interference factor $(1-X)$ where X is the transformed volume fraction. On the other hand, the impingement among the growing particles is more complicated. For instance, the particles are deformed in order to reduce the interfacial energy when two particles are close to each other. The phase-field simulation implicitly considers all the effects taking place in the impingement process. For example, at the time step 50,000 (Fig. 4a), there are few impingements. However, a number of impingements take place after approximately 100,000 time steps.

In summary, a procedure of incorporating diffuse-interface nuclei into phase-field simulations is proposed in this work. The diffuse-interface profiles are generated using the minimax technique, and nuclei are incorporated using Poisson seeding. Nucleation and growth of both a single particle and multi-particles are studied. The critical profiles are compatible with the diffusion description of interfaces in phase-field simulations. The transformation kinetics obtained from the phase-field simulations are in good agreement with traditional theory of particle growth and the KJMA equation. Although illustrative example is on structural transformations, it is also applicable to nucleation and growth involving composition changes and the critical nuclei will automatically satisfy the mass conservation condition. Therefore, the proposed computational procedure is expected to be applicable to any phase transformations and microstructure evolution via nucleation and growth.

The work is supported by the NSF IIP-541674 through the Center for Computational Materials Design (CCMD), NSF DMR-0710483, and NSF DMS-0712744.

[1] L.Q. Chen, Annu. Rev. Mater. Res. 32 (2002) 113.
[2] W.J. Boettinger, J.A. Warren, C. Beckermann, A. Karma, Annu. Rev. Mater. Res. 32 (2002) 163.
[3] L. Granasy, T. Pusztai, T. Borzsonyi, G. Toth, G. Tegze, J.A. Warren, J.F. Douglas, J. Mater. Res. 21 (2006) 309.
[4] H. Emmerich, Adv. Phys. 57 (2008) 1.
[5] N. Moelans, B. Blanpain, P. Wollants, Calphad 32 (2008) 268.
[6] I. Steinbach, Model. Simul. Mater. Sci. Eng. 17 (2009) 073001.
[7] R. Kubo, Rep. Prog. Phys. 29 (1966) 255.
[8] E.M. Lifshitz, L.P. Pitaevskii, Statistical Physics: Part I. Landau and Lifshitz Course of Theoretical Physics, vol. 5, third ed., Pergamon Press, Oxford, 1980.
[9] J.P. Simmons, C. Shen, Y. Wang, Scr. Mater. 43 (2000) 935.
[10] J.P. Simmons, Y. Wen, C. Shen, Y.Z. Wang, Mater. Sci. Eng. A 365 (2004) 136.
[11] D.Y. Li, L.Q. Chen, Scr. Mater. 37 (1997) 1271.
[12] V. Vaithyanathan, L.Q. Chen, Acta Mater. 50 (2002) 4061.
[13] Y. Wang, A.G. Khachaturyan, Acta Mater. 45 (1997) 759.
[14] A. Artemev, Y. Jin, A.G. Khachaturyan, Acta Mater. 49 (2001) 1165.
[15] H.I. Aaronson, J.K. Lee, in: H.I. Aaronson (Ed.), Lectures on the Theory of Phase Transformations, TMS, New York, 1975.
[16] J.Z. Zhu, T. Wang, A.J. Ardell, S.H. Zhou, Z.K. Liu, L.Q. Chen, Acta Mater. 52 (2004) 2837.
[17] B. Wang, Y.H. Wen, J. Simmons, Y. Wang, Metall. Mater. Trans. A 39A (2008) 984.
[18] Y.H. Wen, J.P. Simmons, C. Shen, C. Woodward, Y. Wang, Acta Mater. 51 (2003) 1123.
[19] J.W. Cahn, J.E. Hilliard, J. Chem. Phys. 28 (1958) 258.
[20] J.W. Cahn, J.E. Hilliard, J. Chem. Phys. 31 (1959) 688.
[21] Y.A. Chu, B. Moran, A.C.E. Reid, G.B. Olson, Metall. Mater. Trans. A 31A (2000) 1321.
[22] L. Zhang, L.Q. Chen, Q. Du, Phys. Rev. Lett. 98 (2007) 265703.
[23] L. Zhang, L.Q. Chen, Q. Du, Acta Mater. 56 (2008) 3568.
[24] L. Zhang, L.Q. Chen, Q. Du, J. Sci. Comput. 37 (2008) 89.
[25] L. Zhang, L.Q. Chen, Q. Du, Commun. Comput. Phys. 7 (2010) 674.
[26] P. Rabinowitz, Minimax Methods in Critical Point Theory with Applications to Differential Equations, American Mathematical Society, Providence, RI, 1986.
[27] J. More, T. Munson, Math. Program. 100 (2004) 151.
[28] W.E, W. Ren, E. Vanden-Eijnden, Phys. Rev. B 66 (2002) 052301.
[29] W.E, W. Ren, E. Vanden-Eijnden, J. Chem. Phys. 126 (2007) 164103.
[30] L. Granasy, T. Borzsonyi, T. Pusztai, Phy. Rev. Lett. 88 (2002) 206105.
[31] S.M. Allen, J.W. Cahn, Acta Metall. 27 (1979) 1085.
[32] D. Fan, L.Q. Chen, Philos. Mag. Lett. 75 (1997) 187.
[33] A.N. Kolmogorov, Izv. Akad. Nauk: Ser. Mat. 1 (1937) 355–359.
[34] W.A. Johnson, R.F. Mehl, Trans. AIME 135 (1939) 416.
[35] M. Avrami, J. Chem. Phys. 7 (1939) 1103.
[36] M. Avrami, J. Chem. Phys. 8 (1940) 212.
[37] M. Avrami, J. Chem. Phys. 9 (1941) 177.